

# **Characterization of Amorphous Silicon Thin Films and PV Devices**

**Phase I Annual Technical Report  
January 1998 — January 1999**

P.C. Taylor  
*Department of Physics  
University of Utah  
Salt Lake City, Utah*



**NREL**

**National Renewable Energy Laboratory**

1617 Cole Boulevard  
Golden, Colorado 80401-3393

NREL is a U.S. Department of Energy Laboratory  
Operated by Midwest Research Institute • Battelle • Bechtel

Contract No. DE-AC36-98-GO10337

# Characterization of Amorphous Silicon Thin Films and PV Devices

Phase I Annual Technical Report  
January 1998 — January 1999

P.C. Taylor  
*Department of Physics  
University of Utah  
Salt Lake City, Utah*

NREL Technical Monitor: B. von Roedern

Prepared under Subcontract No. XAK-8-17619-13



**NREL**

**National Renewable Energy Laboratory**

1617 Cole Boulevard  
Golden, Colorado 80401-3393

NREL is a U.S. Department of Energy Laboratory  
Operated by Midwest Research Institute • Battelle • Bechtel

Contract No. DE-AC36-98-GO10337

## NOTICE

This report was prepared as an account of work sponsored by an agency of the United States government. Neither the United States government nor any agency thereof, nor any of their employees, makes any warranty, express or implied, or assumes any legal liability or responsibility for the accuracy, completeness, or usefulness of any information, apparatus, product, or process disclosed, or represents that its use would not infringe privately owned rights. Reference herein to any specific commercial product, process, or service by trade name, trademark, manufacturer, or otherwise does not necessarily constitute or imply its endorsement, recommendation, or favoring by the United States government or any agency thereof. The views and opinions of authors expressed herein do not necessarily state or reflect those of the United States government or any agency thereof.

Available to DOE and DOE contractors from:  
Office of Scientific and Technical Information (OSTI)  
P.O. Box 62  
Oak Ridge, TN 37831  
Prices available by calling 423-576-8401

Available to the public from:  
National Technical Information Service (NTIS)  
U.S. Department of Commerce  
5285 Port Royal Road  
Springfield, VA 22161  
703-605-6000 or 800-553-6847  
or  
DOE Information Bridge  
<http://www.doe.gov/bridge/home.html>



## Table of Contents

1.	Introduction	3
2.	Second Harmonic Detection of ESR	4
3.	Light-Induced Defects in a-Si <sub>x</sub> :H Alloys	8
4.	Low Temperature Kinetics of Band-Tail Carriers	13
5.	NMR Studies of Molecular Hydrogen	17
6.	Conclusions	17
7.	References	17
8.	Publications	19

## 1. INTRODUCTION

### Objectives

The major objectives of this subcontract are (1) to prepare new materials based on hydrogenated amorphous silicon (a-Si:H), (2) to characterize the important defects and impurities in the bulk and at surfaces and interfaces, (3) to identify metastabilities and to determine if the metastabilities that plague devices are "intrinsic" or "extrinsic", (4) to obtain a better understanding of how defects affect device performance.

### Approaches

Two major approaches are utilized both (1) to improve the understanding of metastabilities in a-Si:H, alloys based on a-Si:H, microcrystalline alloys, and devices and (2) to develop schemes to mitigate the deleterious metastabilities in these materials and devices. First, novel alloys, such as those containing sulfur or selenium, are grown and characterized. Special emphasis is placed on understanding how impurities affect the electronic properties of such alloys and of devices based on such alloys. Second, a wide array of characterization techniques is employed to study the optical and electronic properties. The optical techniques include optical absorption as measured using photo-thermal deflection spectroscopy (PDS), photoluminescence (PL), PL excitation spectroscopy, optically detected or optically pumped electron spin resonance (ESR) and other spectroscopies using a wide range of optical sources. The major magnetic resonance technique is ESR. The transport techniques are photoconductivity (PC) and the constant photocurrent method (CPM).

### Research Tasks

The subcontract is divided into two tasks. One task is the growth of doped and undoped a-Si:H and related alloys. Alloys with concentrations of group VI elements, such as sulfur or selenium, have been found to exhibit very inefficient, n-type doping, and the potential of sulfur [see publications 1-4] and selenium [see publication 5] alloys for photovoltaic applications has been investigated. The plasma assisted chemical vapor deposition (PECVD) system has been upgraded to a three-chamber system capable of making state-of-the-art films and devices.

A second task is the characterization of a-Si:H and related alloys and devices. We have been using photoconductivity (PC) [see publication 6], photoluminescence excitation (PLE) spectroscopy, time resolved PL, optically detected magnetic resonance (ODMR), electron spin resonance (ESR) [see publications 7-9], and spin-dependent photoinduced absorption (PADMR) [see publication 10] to probe defects which produce absorption below the gap in a-Si:H. A review of some of the most recent results is available elsewhere [see publication 11].

Perhaps the most significant result of the past year is the use of second harmonic detection of ESR and optically induced ESR (LESR) in a-Si:H and related alloys. This new technique provides an increase in the signal-to-noise ratios of more than three orders of magnitude and allows defects in a-Si:H to be studied at concentrations much lower than possible previously.

## 2. SECOND HARMONIC DETECTION OF ESR

Electron spin resonance (ESR) and light-induced ESR (LESR) in a-Si:H have been studied for many years. In the dark there exists an ESR resonance at  $g = 2.0055$  and a peak-to-peak linewidth of the usual derivative spectrum of  $\Delta H_{pp}$  of about 7.5 G. This spectrum is attributed to a silicon dangling-bond defect. Below 40 K these dangling-bond defects are very difficult to observe because of a technical difficulty known as microwave-power saturation. For this reason we have perfected a “rapid passage” technique to increase the sensitivity of these measurements. To test this technique we have measured the LESR at about 40 K. In LESR two additional signals appear, a broad line at  $g = 2.01$  with  $\Delta H_{pp} \approx 20$  G and a narrow line at  $g = 2.004$  with  $\Delta H_{pp} \approx 6$  G. The broad line has been assigned to holes trapped in the valence-band tail and the narrow line to electrons trapped in the conduction-band tail. Prior to our recent results there were no detailed kinetic measurements of the low-temperature LESR in a-Si:H. The reason that detailed measurements were not performed previously is simply that the ordinary derivative detection technique does not provide sufficient signal-to-noise ratios. However, using the second-harmonic technique the saturation of the LESR (and also of the dark ESR) signal with increasing microwave power is drastically reduced. With this technique we have measured the LESR lineshapes and kinetics over a wide range of excitation intensities.

Figure 1a shows a second-harmonic LESR spectrum measured at 40 K using 20 mW microwave power. At this microwave power the normal derivative signal would be greatly reduced due to saturation effects. As a comparison, the integral of a low-microwave-power (2  $\mu$ W), first-harmonic spectrum is shown in Fig. 1b. It is clear that the lineshapes of the two spectra are very similar, although certainly not identical. The smooth lines in Fig. 1 are fits with two Gaussian distributions.

The ratio of the broad line to the narrow line is larger in the second-harmonic spectrum. This phenomenon is caused by the different saturation behaviors of the broad and narrow lines in the two detection schemes. It is not easy to get an accurate measurement of the spin density using only the second-harmonic detection, but one can accurately measure spin densities using the second-harmonic detection scheme if the signals are tied to unsaturated measurements of the signal using the ordinary detection scheme. In this way one may measure dark ESR spin densities that are well below  $10^{16}$   $\text{cm}^{-3}$  at low temperatures provided that the samples are thick enough so that the ESR is not dominated by spins at surface states.

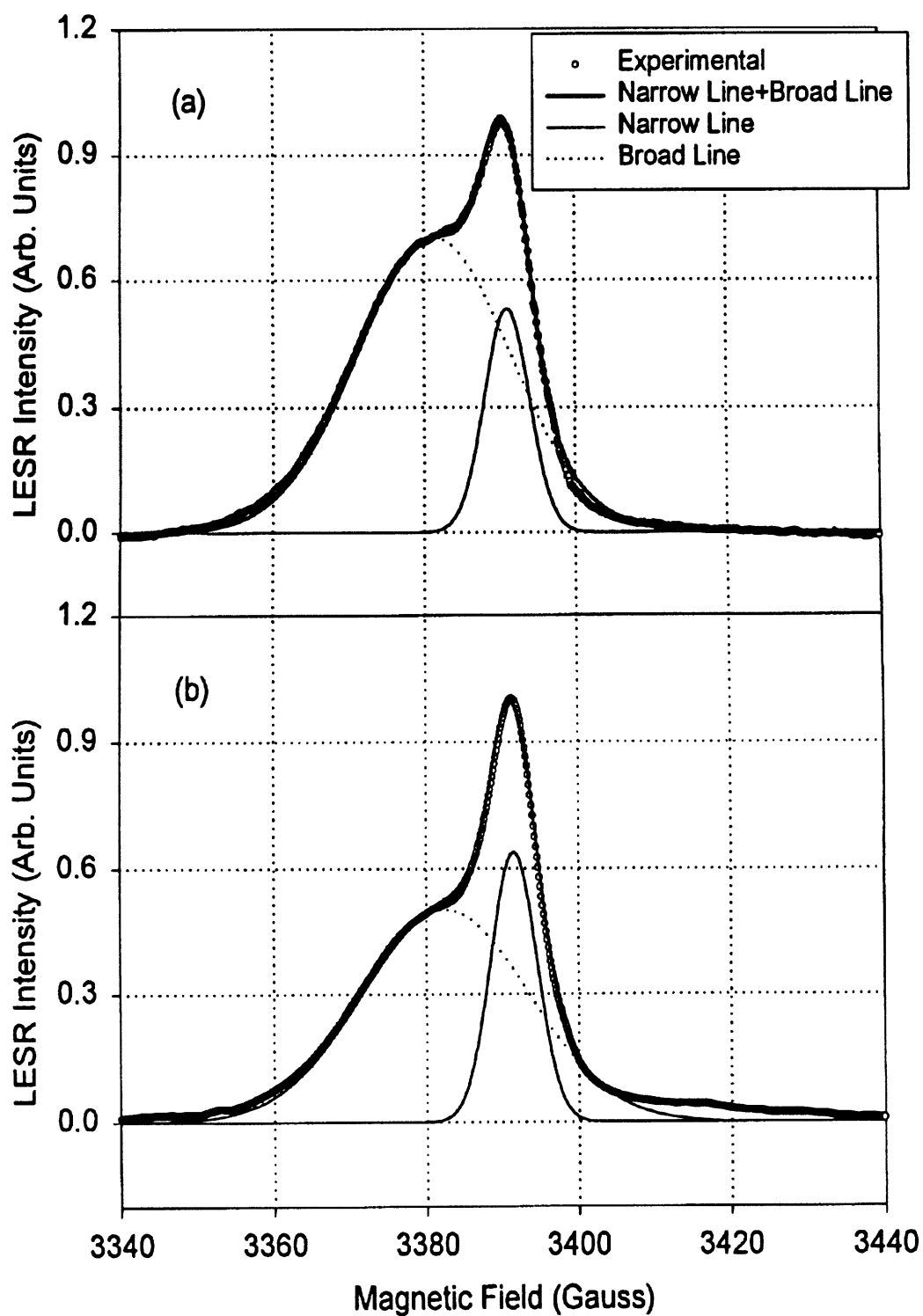


Fig. 1. (a) LESR spectrum measured by second harmonic detection with 20 mW microwave power; (b) Integral of a first harmonic spectrum measured with 2  $\mu$ W microwave power. The smooth lines are fits with Gaussian distributions. Both spectra were measured at 40 K with 12 mW/cm<sup>2</sup> excitation intensity.

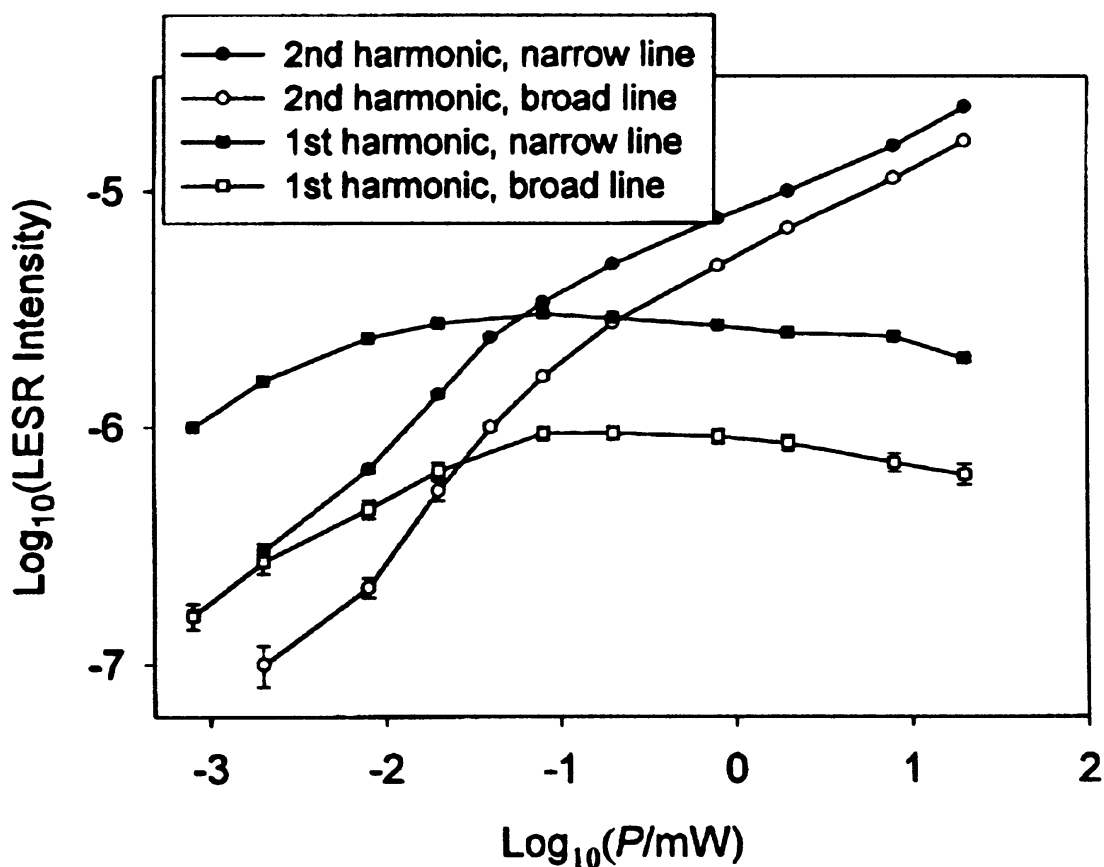


Fig. 2. LESR intensity versus microwave power ( $P$ ). The first-harmonic data were measured using peak-to-peak heights of the derivative spectra and the second-harmonic data were measured using peak heights of the absorption spectra from the base line.

Figure 2 shows that at 40 K the second-harmonic signal does not saturate appreciably with increasing microwave power even though the first-harmonic signal is very easily saturated. The magnitude of the second-harmonic signal grows roughly linearly with increasing microwave magnetic field (roughly as the square root of the microwave power). At low microwave fields the dependence is slightly super-linear while at high microwave fields the dependence becomes slightly sub-linear. This behavior is expected theoretically [1].

The increase of the narrow line with increasing microwave power is slower than the increase of the broad line, a fact that leads to the relative suppression of the narrow line in Fig. 1a. Figure 2 also shows the extensive saturation of the first harmonic signal. It is clear from Fig. 2 that at 40 K the first harmonic signal is partially saturated even at the lowest attainable microwave powers. In addition, the saturation occurs much more easily for the narrow line than

for the broad line. Since saturation is always a problem at this temperature, one may easily underestimate the intensity in the narrow line using the commonly employed first-harmonic-detection scheme. There is some evidence for such an underestimate in the literature [2].

Even though it is not central to the solution of problem of eliminating the metastabilities in a-Si:H films and PV devices, whether or not there exist significant numbers of charged defects in a-Si:H is an important question. From the defect pool model [3] it has been suggested that the density of charged dangling-bond defects is considerably greater than that of the neutral defects, even in device-quality a-Si:H. Some recent measurements also tend to confirm this suggestion [2, 4, 5, 6]. Some of these conclusions have been based on the ratio of the spin densities in the broad and narrow lines of the LESR. Although the detailed reasons are not clear, it is well known that the LESR measurements only measure a fraction of the light-induced carriers in the band tails. Fast geminate recombination and short spin-spin relaxation times are clearly two important reasons why no LESR is observed for carriers trapped in shallow band-tail states. Probably only deeply trapped carriers exhibit LESR because the localization lengths decrease with increasing trapping energy. Because we do not know what energy distinguishes whether the trapped carriers yield a LESR signal, and furthermore we do not have any reason to assume that these energies are the same for trapped electrons and trapped holes, we may not expect that the spin density of the broad line would be equal to that of the narrow line, even in the absence of artifacts such as microwave saturation or of charged defects. Therefore, to postulate the existence of charged defects based solely on the LESR results is unfounded. In addition, subtle saturation effects, even in the second-harmonic-detection case, may also influence the accuracy of the decomposition into trapped electrons and trapped holes.

We have employed the second-harmonic detection scheme described above to measure the dark ESR spin densities in samples of a-Si:H made with and without hydrogen dilution as supplied by the group of C. R. Wronski at Penn State University. Samples were measured before and after light soaking for about 20 hours with approximately 300 mW/cm<sup>2</sup> of filtered white light from an ELH lamp. Spin densities were calibrated using a weak pitch standard and the usual first-harmonic (derivative of absorption) detection mode.

**Table 1. ESR Spin Densities in Selected Samples from Penn State University**

Sample No.	Thickness (μm)	$N_s$ (as deposited) (cm <sup>-2</sup> )	$N_s$ (annealed) (cm <sup>-2</sup> )	$N_s$ (light soaked) (cm <sup>-2</sup> )	Remarks
LJ69	1.8	$1.9 \pm 0.5 \times 10^{12}$			No dilution
LJ70	1.35	$1.7 \pm 0.5 \times 10^{12}$	$1.7 \pm 0.5 \times 10^{12}$	$1.0 \pm 0.1 \times 10^{13}$	No dilution
LJ71	0.85	$1.1 \pm 0.5 \times 10^{12}$			No dilution
LJ82	0.85	$4.2 \pm 0.5 \times 10^{12}$	$4.2 \pm 0.5 \times 10^{12}$	$9.2 \pm 0.5 \times 10^{12}$	H <sub>2</sub> dilution

Because we obtained a set of samples of different thicknesses (see Table 1) for the case of no hydrogen dilution, we are able to extract both the surface and bulk spin densities unambiguously for these samples. The surface spin density for this set of three samples is  $5 \times 10^{11} \text{ cm}^{-2}$ , and the bulk spin density as deposited is  $1.0 \pm 0.5 \times 10^{16} \text{ cm}^{-3}$ . The two samples that were light-soaked were annealed at  $180^\circ \text{ C}$  for four hours in a nitrogen atmosphere before irradiation. As shown in Table 1, this annealing had no effect on the dark ESR spin densities. Because there was only a single sample in the hydrogen-diluted case, we cannot separate the surface and bulk contributions to the spin density unambiguously; however, the measured densities are large enough that we strongly suspect that they represent bulk spin densities. [The calculated surface spin densities are about an order of magnitude too large to be realistic.] If we assume that the spin densities for the hydrogen-diluted sample are entirely due to bulk spins, then the densities calculated from Table 1 are  $5.6 \times 10^{16} \text{ cm}^{-3}$  and  $1.1 \times 10^{17} \text{ cm}^{-3}$  for the as-deposited and light-soaked states, respectively. For the two samples of the same thickness ( $0.85 \mu\text{m}$ ), the dark spin density for the hydrogen diluted sample is approximately four times greater than for the undiluted sample. It is difficult to discern the significance of this difference for only one pair of samples.

These results show that hydrogen dilution does not significantly affect the optically induced production of neutral silicon dangling bonds even though there appears to be an improvement in the stability of cells made using the hydrogen-dilution process. Further experiments on both cells and individual layers are necessary to confirm this conclusion.

### 3. LIGHT-INDUCED DEFECTS IN $\text{a-SiS}_x\text{:H}$ ALLOYS

One approach to removing the deleterious metastabilities that are known loosely and collectively as the Staebler-Wronski effect is the addition of chalcogen elements (S and Se) into  $\text{a-Si:H}$ . This approach has resulted in a decrease of the degradation of conductivity and photoconductivity after light-soaking. Wang et al. [7] found a persistent photoconductivity (PPC) in  $\text{a-SiS}_x\text{:H}$  films, whose effect on both the conductivity and photoconductivity is opposite to the Staebler-Wronski effect. It is possible that the presence of the PPC effect may increase the stability of the materials and devices.

Recent studies have shown that the Staebler-Wronski effect and the PPC effect occur on different time scales during light-soaking and anneal at different temperatures in  $\text{a-SiS}_x\text{:H}$  and  $\text{a-SiSe}_x\text{:H}$  [see publication 12]. A similar phenomenon has also been observed in compensated  $\text{a-Si:H}$  samples doped with phosphine and diborane [8]. Although a model based on optically-induced activation of sulfur donors during light-soaking has been proposed [9], there is still only weak experimental evidence to support the model. Sulfur can be a double donor in crystal silicon, and the lowest donor level is relatively deep [10]. In addition sulfur donors can be passivated by hydrogen atoms. The situation is more complicated in the amorphous phase. First, the random network in amorphous silicon provides the possibility for chalcogen atoms to form two-fold-coordinated structures (the favorite coordination of chalcogen atoms), which is one factor that leads to the low efficiency of doping [11]. Second, the significant concentration of hydrogen in the materials may passivate the donors that are at substitutional sites.

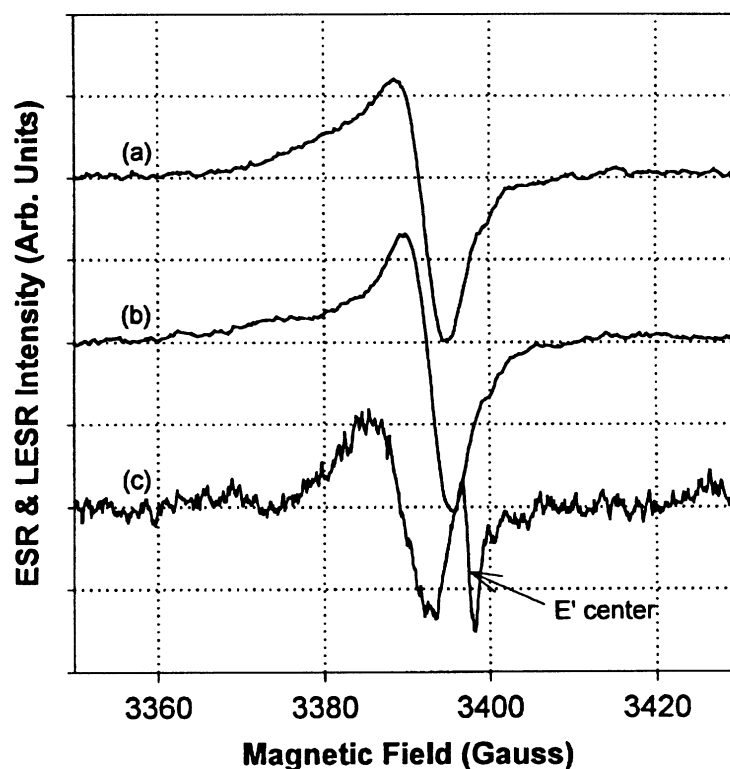


Fig. 3. ESR and LESR spectra of a-SiS<sub>x</sub>:H. The LESR spectra [(a) and (b)] were measured at 40 K with 8 μW of microwave power. (a) 2 at. % of sulfur and (b) 0.6 at. % of sulfur. The ESR spectrum (c) was measured at room temperature with 20 μW of microwave power for the sample with 0.6 at. % of sulfur.

During the past quarter we have measured the kinetics of generation and annealing of light-induced defects in a-SiS<sub>x</sub>:H films and in undoped a-Si:H films. The defect density was measured by electron spin resonance (ESR) and light-induced ESR (LESR) techniques.

Figure 3 shows some examples of the ESR and LESR in a-SiS<sub>x</sub>:H, where the feature labeled E' center is from the quartz Dewar. The dark ESR spectrum is for a sample with 0.6 at. % sulfur after ten days light-soaking at 300 K. For this spectrum the dark spin density is  $8 \times 10^{16}$  cm<sup>3</sup>. The g value of 2.0055 and the width of 7 to 8 G confirm that the dark ESR spectrum comes from silicon dangling bonds. The LESR spectra change with sulfur concentration. The broad line (observed at  $g \approx 2.01$  for undoped a-Si:H) gradually disappears with increasing sulfur concentration as reported in a previous paper [12], and at the same time the LESR spin density increases [12]. The asymmetry of the LESR line for the sample with high sulfur concentration may be caused by an asymmetry in the g tensor or the spectrum may include more than one line. After comparison with the Se-alloyed sample, we believe that the LESR may come from defects (or traps) related to chalcogen atoms since the LESR spectra of a-SiSe<sub>x</sub>:H are broader than those of a-SiS<sub>x</sub>:H by a factor of 2 to 3. This increase in width from S to Se is expected if the width is due to g anisotropies that result from spin-orbit coupling. The spin-orbit coupling constant for atomic Se is approximately three times that for S.

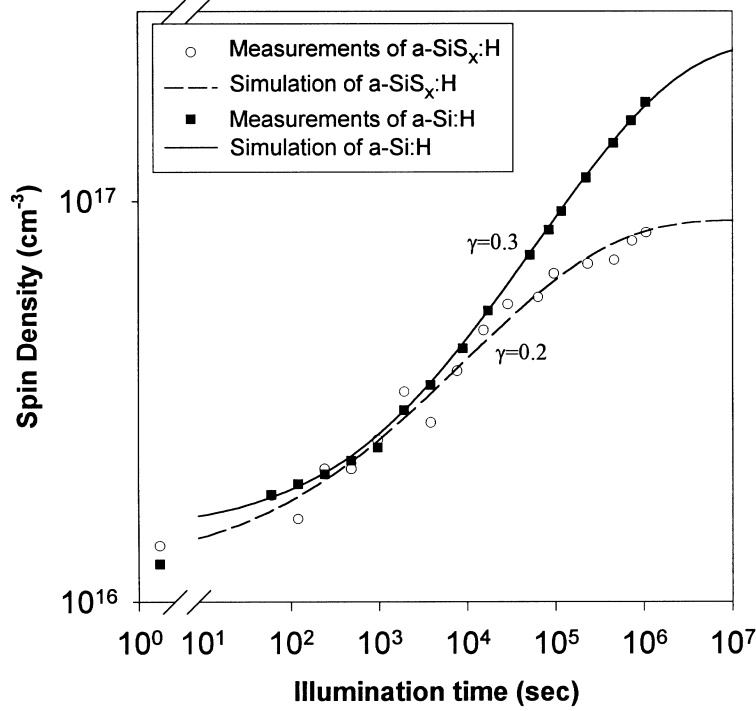


Fig. 4. Kinetics of light-induced defect generation for undoped a-Si:H and a-SiS<sub>x</sub>:H ( $x = 6 \times 10^{-3}$ ). The smooth lines are fits to the experimental data (symbols) with Eq. (1) with the parameters:  $N_0 = 1.2 \times 10^{16} \text{ cm}^{-3}$ ,  $N_S = 9 \times 10^{16} \text{ cm}^{-3}$ ,  $\tau_g = 8 \times 10^4 \text{ s}$  and  $\beta = 0.38$  for a-SiS<sub>x</sub>:H ( $x = 6 \times 10^{-3}$ );  $N_0 = 1.5 \times 10^{16} \text{ cm}^{-3}$ ,  $N_S = 2.5 \times 10^{17} \text{ cm}^{-3}$ ,  $\tau_g = 8 \times 10^5 \text{ s}$  and  $\beta = 0.45$  for a-Si:H

The generation kinetics of light-induced silicon dangling bonds in an a-SiS<sub>x</sub>:H film (0.6 at. % S) and an undoped a-Si:H film are displayed in Fig. 4, where the symbols are experimental data and the lines are the fits to a stretched-exponential function [13],

$$N(t) = N_S - (N_S - N_0) \exp \left[ - \left( \frac{t}{\tau_g} \right)^\beta \right], \quad (1)$$

where,  $N_S$  is the saturated value,  $N_0$  the initial value,  $\tau_g$  the inducing time and  $\beta$  the dispersion coefficient. The parameters for the best fits to the experimental data appear in the caption of Fig. 4. Even though the initial values are roughly the same for the two samples, the saturated value is lower for the a-SiS<sub>x</sub>:H sample ( $x \approx 10^{-3}$ ) than for the undoped sample. Meanwhile, the dispersion coefficient,  $\beta$  is smaller for a-SiS<sub>x</sub>:H than for undoped a-Si:H. Correspondingly, the approximate slope in the region of steepest ascent on a log-log plot ( $\gamma$  in Fig. 4) decreases from the usual value of 0.3 to approximately 0.2.

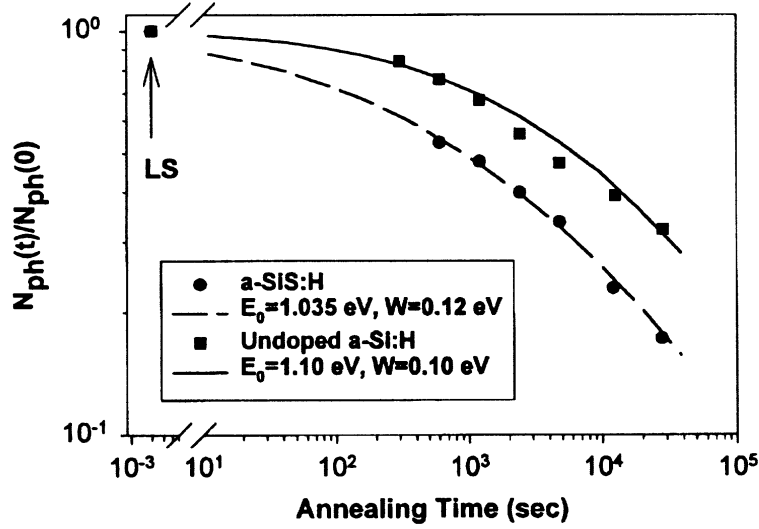


Fig. 5. Kinetics of light-induced defect annealing for undoped a-Si:H and a-SiS<sub>x</sub>:H ( $x = 6 \times 10^{-3}$ ). The smooth lines are fits to the experimental data with Eqs. (2) through (4) with the parameters:  $E_0 = 1.035$  eV,  $W = 0.12$  eV for a-SiS<sub>x</sub>:H ( $x = 6 \times 10^{-3}$ );  $E_0 = 1.10$  eV,  $W = 0.10$  eV for a-Si:H.

Figure 5 shows the annealing kinetics of light-induced defects at 120°C. Clearly the light-induced defects are more easily annealed away in a-SiS<sub>x</sub>:H than in a-Si:H. Based on the defect model of Hata and Wagner [14], there is a distribution of annealing activation energies ( $E_a$ ). The defects with lower  $E_a$  anneal first, and the ones with higher  $E_a$  live longer. If the distribution of  $E_a$  is a Gaussian distribution, then

$$N(E_a) = \frac{N'_s}{(2\pi W^2)^{1/2}} \exp\left(-\frac{(E_a - E_0)^2}{2W^2}\right), \quad (2)$$

where  $N'_s$  is the initial value of the light-induced defects,  $E_0$  the center and  $W$  the width of the distribution. The light-induced defect density remaining after annealing at a temperature  $T$  for a time  $t$  is

$$N(t) = \int_0^\infty N(E_a) \exp\left(-\frac{t}{\tau(E_a, T)}\right) dE_a, \quad (3)$$

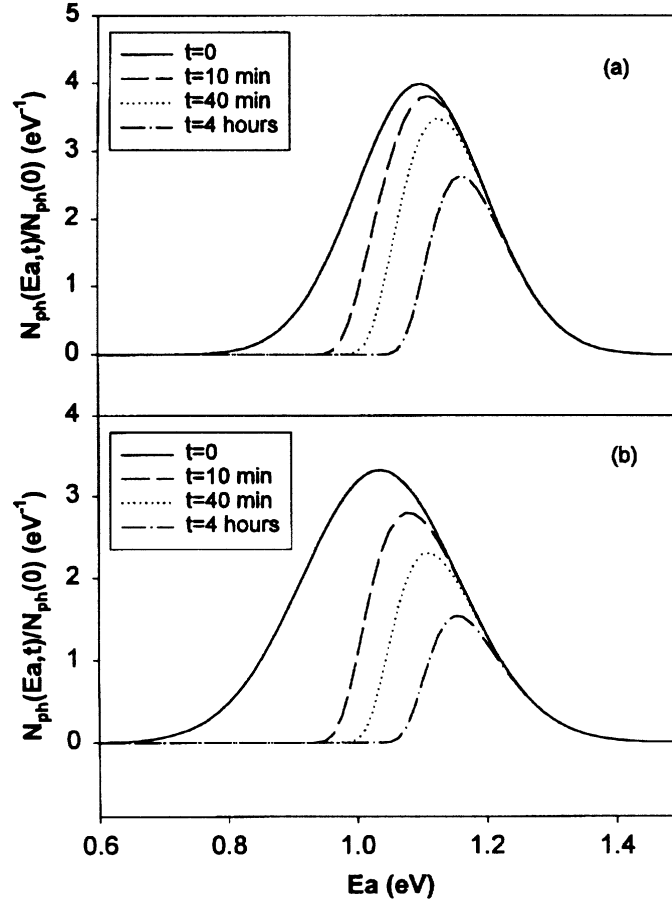


Fig. 6. Distribution of annealing activation energies with varied annealing times for (a) undoped a-Si:H and (b) a-SiS<sub>x</sub>:H ( $x = 6 \times 10^{-3}$ ).

The solid lines in Fig. 5 are the calculations using Eqs. (2) through (4). The parameters for the

$$\tau(E_a, T) = \tau_0 \exp\left(\frac{E_a}{kT}\right), \quad (4)$$

best fits to the experimental data are  $E_0 = 1.035$  eV,  $W = 0.12$  eV for a-SiS<sub>x</sub>:H ( $x = 0.6$  at. %) and  $E_0 = 1.10$  eV,  $W = 0.10$  eV for a-Si:H. Although the difference between the most probable activation energies is small for the two samples, this difference results in a significant change in annealing behaviors as indicated in Fig. 6. In this figure the curves show the distributions of  $E_a$  for the centers remaining after certain annealing times.

The incorporation of sulfur into amorphous silicon changes the structure of the material. Compared with undoped a-Si:H, the slower generation of light-induced defects is probably due to thermal annealing or to light-induced annealing during the light-soaking process. The kinetics governing the net generation of defects are a competition between generation and annealing.

Therefore, if the generation rates are the same, the higher the annealing rate, the lower the saturated defect density. The experimental results confirm this scenario because the annealing activation energy is lower in a-SiS<sub>x</sub>:H than in a-Si:H. Some recent studies show there are macroscopic changes occurring during light-soaking and annealing [15]. The low annealing activation energy in a-SiS<sub>x</sub>:H may indicate that the network in this material is more flexible than in a-Si:H. This presumption is reasonable since the chalcogen atoms easily form two-fold-coordinated structures, such as occur in the standard chalcogenide glasses. Two-fold-coordinated structures may provide more flexibility to the underlying tetrahedral structure.

The dark ESR spectrum at 300 K, both before and after light soaking, shows only the signature of silicon dangling bonds, which means the defects related to sulfur, if any, are not ESR active at this temperature. The increase of the low-temperature LESR with increasing sulfur concentration (the same trend happens to a-SiSe<sub>x</sub>:H) suggests that the LESR signal may result from S-related defects, at least for the samples with high sulfur concentrations. One may speculate that either the S-related defects are in their charged states in the dark, as is the case in the chalcogenide glasses, or the S-related defects are passivated by the presence of hydrogen atoms, as can occur in crystalline silicon. Experimentally we did not find any change in the low-temperature LESR spectra or spin densities after prolonged light-soaking at 300 K. This fact indicates that there is no obvious increase in the S-related defects upon light soaking and confirms that any model for the sulfur-related LESR must involve the rearrangement of charge (or perhaps also of hydrogen atoms) at existing defect sites rather than the creation of new defects.

#### 4. LOW TEMPERATURE KINETICS OF BAND-TAIL CARRIERS

In 1989 Shklovskii [16] discovered that at low temperatures the simultaneous diffusion and recombination of electron-hole pairs in amorphous semiconductors is a universal property that does not depend on the functional form for the density of localized electronic states. This generality has prompted renewed interest [17] in the diffusion and recombination mechanisms for electrons and holes trapped in localized band-tail states in hydrogenated amorphous silicon (a-Si:H), the quintessential amorphous semiconductor. We have measured the generation and recombination kinetics for band-tail electrons and holes in a-Si:H. These measurements employ a novel electron spin resonance (ESR) technique [second-harmonic detection of SH-ESR as described in the Quarterly Progress report for the first quarter of phase I] that surpasses the sensitivity of previous measurements [2, 18] by over three orders of magnitude. This increased sensitivity improves by orders of magnitude the lower bound on photo-excited carrier concentrations above which non-geminate (distant pair) recombination dominates the recombination process in tetrahedrally coordinated amorphous semiconductors [16, 19]. Also, these measurements test the universality of the diffusion and recombination of photo-excited electrons and holes in amorphous semiconductors at orders of magnitude lower carrier densities and orders of magnitude longer recombination times. Using SH-ESR the kinetics can be extracted for saturated spin densities as low as  $5 \times 10^{14} \text{ cm}^{-3}$ .

In hydrogenated amorphous silicon (a-Si:H) two optically induced electron spin resonance (LESR) signals are commonly observed at temperatures below about 100 K. These two signals, whose characteristic g-values are approximately 2.004 and 2.01, are usually

attributed to electrons trapped in localized conduction-band-tail states and holes trapped in localized valence-band-tail states, respectively [20]. Recently, using pulsed LESR measurements in samples of a-Si:H with different concentrations of  $^{29}\text{Si}$ , Umeda et al. [17] have determined that the wave function of the trapped electrons is consistent with an antibonding orbital highly localized at a single Si-Si bond. These authors also speculated that the hole was similarly localized at a single Si-Si bond. In addition to these two LESR signals, there is a third, metastable ESR signal centered at  $g = 2.0055$  that is attributed to neutral silicon dangling bonds [21]. Because of the small difference in  $g$ -values, it is often difficult to separate this latter signal from that attributed to band-tail electrons.

Films of nominally undoped a-Si:H were deposited on ESR-grade quartz substrates using a standard PECVD technique. These films, which were  $3\ \mu\text{m}$  thick, had bulk ESR spin densities less than  $5 \times 10^{15}\ \text{cm}^{-3}$ . Five samples were stacked together to perform the LESR experiments. [The high-Q ESR cavity is an effective light reflector allowing the incident light to be absorbed essentially uniformly, even with five films stacked together.] Before measurement, the samples were annealed at 468 K in a dry nitrogen atmosphere for two hours and then slowly cooled to 300 K. Samples were cooled from 300 K to 40 K in the dark. ESR and LESR measurements were performed on a Bruker 200D-SRC spectrometer at 9.5 GHz. Variable temperatures, accurate to  $\pm 1\ \text{K}$ , were obtained using a Helitran flow system. The excitation source was a He-Ne laser (1.96 eV). Light intensities at the sample were varied from  $2 \times 10^{-6}\ \text{mW/cm}^2$  to  $12\ \text{mW/cm}^2$  using neutral density filters. All spectra were taken with 2 G modulation amplitude.

The LESR spectra were obtained using a "rapid passage" technique that employs second harmonic detection (SH-LESR). Because of the long spin-lattice relaxation times ( $T_1$ ) in a-Si:H at low temperatures ( $T \lesssim 100\ \text{K}$ ), this technique provides an effective increase in the sensitivity of detection for the LESR of up to three orders of magnitude over the standard first harmonic detection [see publication 9]. These results employ the absorption component of the SH-LESR because the dispersion component contains greater noise [22]. A Fourier transformation of the Bloch equations [23] shows that the second harmonic absorption signal is a sum of even derivatives, including the absorption itself (zeroth derivative). Under the present rapid passage conditions, which are sometimes referred to as "nearly sudden passage" [24], the absorption term dominates. This situation occurs when  $\omega T_1 \gg 1$ , where  $\omega$  is the modulation frequency of the magnetic field ( $2\pi \times 50\ \text{kHz}$  in the present experiment) and  $T_1 \approx 1\ \text{ms}$  at 30 K [17]. The major complication with the SH-LESR technique is that, in addition to the usual ESR parameters, the spin density depends subtly on  $T_1$ . For this reason one must carefully compare spectra to known absorption signals to obtain accurate measurements of the spin densities. For this purpose, we have used the standard LESR in a-Si:H at high spin densities.

As a representative of the SH-LESR technique, we show in Fig. 7 the growth of the signal at 40 K for an excitation intensity of  $2.2 \times 10^{-4}\ \text{mW/cm}^2$ . This growth curve was obtained by sitting on the peak of the SH-LESR spectrum. Since the band-tail hole (broad) and the band-tail electron (narrow) lines have slightly different values of  $T_1$  at any given temperature, the exact lineshape varies slightly depending on the microwave power employed. In agreement with previous pulsed LESR measurements [17], we find that the electron signal saturates more easily than the hole signal. This small variation in the effective intensities of the band-tail electron and

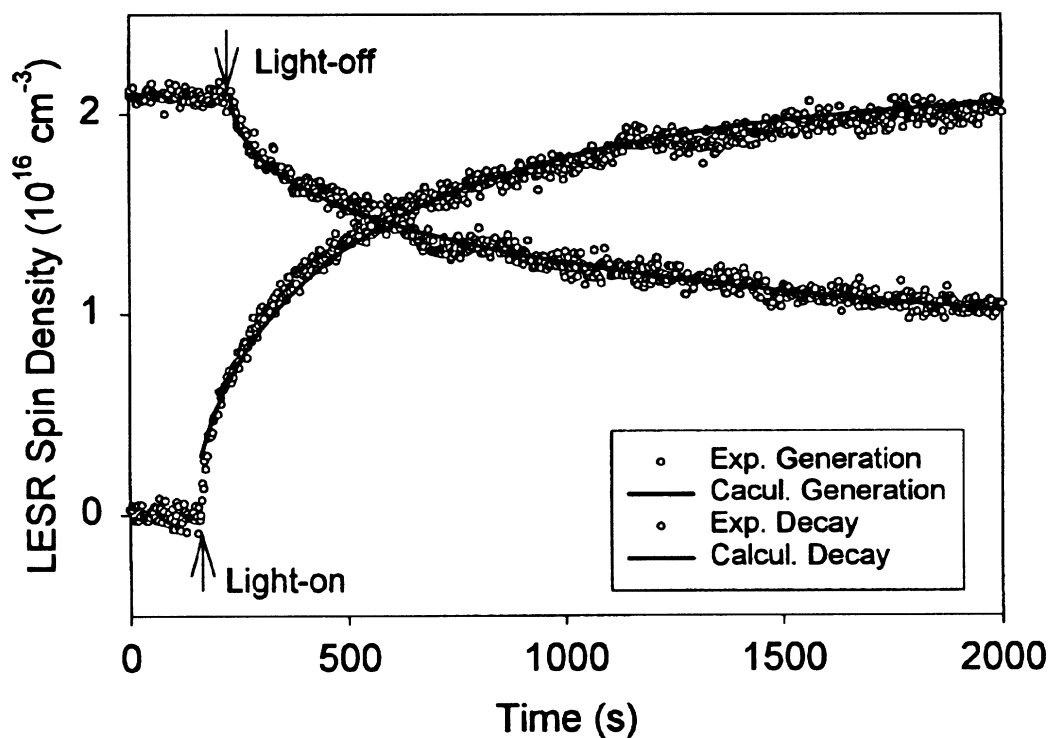


Fig. 7. The generation and decay of the LESR signal with time. The measurements were made using the second-harmonic detection with 20 mW microwave power and  $1.7 \times 10^{-3}$  mW/cm<sup>2</sup> excitation intensity.

band-tail hole signals with microwave power are not important for the present purposes. The decay of the signal after the light is turned off (after approximately 200 s in this representative example) is shown in Fig. 7. The solid lines are fits to the kinetic model described below. [One feature is apparent from Fig. 7: Neither the growth nor the decay can be fit by simple exponential functions. Neither can they be it by simple bimolecular recombination with a unique recombination rate.]

The SH-LESR data can be fit accurately by the simplest phenomenological model that incorporates dispersion [see publication 9]. First, we assume that the LESR results from carriers trapped deeper in their respective band tails than those that recombine quickly ( $< \text{ms}$ ) and primarily contribute to photoluminescence at low temperatures [25, 26]. Although we do not know from these experiments [27] where the demarcation level is that separates the deeper from the shallower traps, we assume the existence of such a level that defines a total number of deeper traps,  $N$ . Since we are at low temperatures ( $T \leq 40$  K for most experiments), we assume that the LESR results from the trapping of carriers that continuously hop down into these deeper states. Finally, we assume that both the generation rates for the LESR and the recombination rates, which presumably involve tunneling, are dispersive. Fitting to the experimental growth and decay curves shows that the dispersion parameters  $\alpha$ , for growth and decay are identical and are independent of excitation intensity within experimental error. We investigated both

monomolecular and bimolecular decay processes and found that at all excitation intensities only the bimolecular decay fits the data. With these assumptions and fitting results, the rate equation for the growth and decay is given by

$$\frac{dN_{\text{LESR}}}{dt} = F(0)(v_1 t)^{-\alpha_1} G(t)[N - N_{\text{LESR}}(t)] - r(0)(v_2 t)^{-\alpha_2} [N_{\text{LESR}}(t)]^2 \quad (5)$$

where, the dispersion parameter for growth or decay is  $\alpha_1 = \alpha_2 = \alpha = 0.5$  for all generation rates. In Eq. (5)  $G(t)$  is the shallowly trapped carrier density that should increase with the excitation intensity,  $F(0)$  is the initial value of the hopping down coefficient,  $r(0)$  is the initial value of the recombination coefficient, and  $v_1$  and  $v_2$  are two parameters with the units of  $\text{s}^{-1}$ . This equation has simple algebraic solutions for both the growth of the SH-ESR after the light has been turned on and the decay from a saturated density after the light has been turn off [see publication 9].

Through the fitting to this phenomenological model we find that, at low temperatures ( $T \lesssim 50$  K), the dispersion is independent of generation rate for generation rates between  $10^{13}$  and  $10^{20} \text{ cm}^{-3} \text{ s}^{-1}$ . Also, the time constants,  $\tau$ , for growth of the SH-ESR depend on the generation rate as  $\tau \propto G^{0.7}$ . Finally, the saturation densities are only weakly dependent on generation rate ( $n_{\text{sat}} \propto G^{0.2}$ ) as shown in Fig. 8. Note that the open circles are the saturation values as determined from the fits to the phenomenological model described above.

Although this fitting clearly identifies the recombination mechanism for the SH-ESR electrons and holes as bimolecular, and therefore non-geminate, there is otherwise little microscopic information to be gained. Fortunately, Shklovski et al. [16] have considered the typical low-temperature creation of electron-hole pairs by the absorption of light. If the carriers are created near the mobility edge, then they readily become trapped in the localized electronic states within the band tails, and at low temperatures they separate by diffusion due to hopping downward in energy. Levin et al. [19] have shown that, even at very low excitation intensities, the dominant recombination mechanism for carriers excited in this fashion is bimolecular, i.e., there is no correlation between the excitation of electron-hole pairs and the ultimate recombination of electrons and holes. This recombination process is sometimes called distant-pair recombination [28]. Levin et al. have shown that the dominant radiative recombination process is distant pair (non-geminate) recombination at generation rates,  $G$ , far below those used in this study (many orders of magnitude below  $G = 10^{17} \text{ cm}^{-3} \text{ s}^{-1}$ , which corresponds to approximately  $10 \mu\text{W}/\text{cm}^2$  for the thicknesses of samples we have employed. In addition, Levin et al. [19] have determined that the equilibrium carrier concentrations in the band tails are proportional to  $G^{0.16}$  and the mean radiative lifetimes,  $\tau$ , are proportional to  $G^{-0.84}$  [19]. Both of these values are consistent with those extracted from our fitting to the SH-LESR at orders of magnitude smaller values of  $G$  and orders of magnitude larger values of  $\tau$  than observed previously by PL or LESR measurements.

## 5. NMR STUDIES OF MOLECULAR HYDROGEN

The measurements of molecular hydrogen are made using nuclear magnetic resonance (NMR). We employ a Jeener-Broekaert pulse sequence [29] and look at the echo following the third pulse. Although we have used this technique to measure local motion of bonded hydrogen [30], this is a new technique for measuring molecular hydrogen and is the first direct measurement of molecular hydrogen at these low concentrations in a-Si:H.

We have measured molecular hydrogen in several hot-wire (HW) samples supplied by Drs. Mahan and Crandall of NREL. These preliminary measurements indicate that the molecular hydrogen in the hot wire material is typically less than that in the PECVD material. Since the hydrogen concentrations in HW films tend to be less than in PECVD films, we do not know whether the concentration of molecular hydrogen is less in HW films than in PECVD films with the same total hydrogen concentrations. We do know that the percentage of hydrogen that exists as molecular hydrogen is less in HW films. [In PECVD films the molecular hydrogen is  $\sim 10\%$  of the total hydrogen concentration while in the HW films we have studied so far the percentages are  $\leq 1.0\%$ .]

## 6. CONCLUSIONS

Major accomplishments of the previous year include (1) an evaluation of the potential for n-type doping of a-SiS<sub>x</sub>:H and a-SiSe<sub>x</sub>:H alloys, (2) an investigation of the optically induced metastabilities in a-SiS<sub>x</sub>:H and a-SiSe<sub>x</sub>:H alloys with regard to their potential use in photovoltaic applications, and (3) a more detailed understanding of the kinetics of light induced ESR due to carriers trapped in localized band-tail states in a-Si:H. Also of importance are preliminary measurements of the defects and metastabilities in hot-wire samples of a-Si:H and in samples of a-Si:H made under strong hydrogen dilution. The preliminary measurements on hydrogen dilution suggest that the production of neutral silicon dangling bonds is not suppressed from the standard material even though there appears to be an improvement in the stability of cells made using the hydrogen-dilution process.

The new three-chamber, load-locked PECVD deposition system is functioning and producing intrinsic and doped films of a-Si:H. Plans for the next year include the production of high quality devices using this new deposition system.

## 7. REFERENCES

1. W. E. Carlos, Naval Research Laboratory, Washington, D. C., private communication.
2. G. Schumm, W. B. Jackson, and R. A. Street, Phys. Rev. **B48**, 14198 (1993).
3. S. C. Deane and M. J. Powell, Phys. Rev. **B48**, 10815 (1993).
4. M. Gunes, C. R. Wronski, and T. J. McMahon, J. Appl. Phys. **76**, 2260 (1994).

5. M. Gunes and C. R. Wronski, *J. Appl. Phys.* **81**, 3526 (1997).
6. V. Nadady, R. Durny, and E. Pincik, *Phys. Rev. Lett.* **78**, 1102 (1997).
7. S. L. Wang, J. M. Viner, M. Anani and P. C. Taylor, *J. Non-Cryst. Solids* **164-166**, 251 (1993).
8. D. Caputo, G. De Cesare, F. Palma, M. Tucci, C. Minarini and E. Terzini, *Mat. Res. Soc. Symp.* **467**, 91 (1997).
9. S. L. Wang and P. C. Taylor, *Solid State Commun.* **95**, 361 (1995).
10. H. G. Grimmeiss and E. Janzen, in *Deep Centers in Semiconductors*, edited by S. T. Pantelides (Gordon and Breach Science Publisher, New York, 1986), p. 87.
11. S. L. Wang, Z. H. Lin, I M. Viner and P. C. Taylor, *Mat. Res. Soc. Symp. Proc.* **336**, 559 (1994).
12. B. Yan and P. C. Taylor, *Mat. Res. Soc. Symp. Proc.* **467**, 103 (1997).
13. D. Redfield and R. H. Bube, *Appl. Phys. Lett.* **54**, 1037 (1989).
14. N. Hata and S. Wagner, *J. Appl. Phys.* **72**, 2857 (1992).
15. H. Fritzsche, *Mat. Res. Soc. Symp. Proc.* **467**, 19 (1997).
16. B. I. Shklovskii, H. Fritzsche, and S.D. Baranovski, *Phys. Rev. Lett.* **62**, 2989 (1989).
17. T. Umeda, S. Yamasaki, J. Isoya, A. Matsuda, and K. Tanaka, *Phys. Rev. Lett.* **77**, 4600 (1996).
18. F. Boulitrop and D. J. Dunstan, *Solid State Commun.* **44**, 841 (1982).
19. E. I. Levin, S. Marianer, and B. I. Shklovskii, *Phys. Rev. B* **45**, 5906 (1992).
20. R. A. Street, D. K. Biegelsen, and R. L. Weisfield, *Phys. Rev. B* **30**, 5861 (1984).
21. The first attribution of this signal to neutral Si dangling bonds is contained in M. H. Brodsky and R. S. Title, *Phys. Rev. Lett.* **23**, 581 (1969).
22. D. D. Thomas, L. R. Dalton, and J. S. Hyde, *J. Chem. Phys.* **65**, 3006 (1976).
23. W. E. Carlos, Jr., private communication.

24. W. Weger, Bell System Tech. J. **39**, 1013 (1960).
25. F. Boulitrop and D.J. Dunstan, J. Non-Cryst. Solids **77 & 78**, 663 (1985).
26. R. A. Street, Adv. Phys. **30**, 593 (1981).
27. We have experiments in progress (N. Schultz and P. C. Taylor) that will measure these demarcation energies as a function of generation rate. These results will be reported later.
28. K. Morigaki, D. J. Dunston, B. C. Cavenett, P. Dawson, J. E. Nicholls, S. Nitta, and K. Shimakawa, Solid State Commun. **26**, 981 (1978).
29. J. Jeener and P. Broekaert, Phys. Rev. **157**, 232 (1967).
30. For examples of the use of the Jeener-Broekaert pulse sequence to measure local hydrogen motion in a-Si:H see P. Hari, P. C. Taylor, and R. A. Street, J. Non-Cryst. Solids **198-200**, 52 (1996) and references contained therein.

## 8. PUBLICATIONS

1. J.-H. Yoon and P. C. Taylor, *J. Non-Cryst. Solids* **227-230**, 385 (1998).
2. J.-H. Yoon, P. C. Taylor, and Czang-Ho Lee, *J. Non-Cryst. Solids* **227-230**, 324 (1998).
3. R. M. Mehra, Jasmina, P. C. Mathur, and P. C. Taylor, *Thin Solid Films* **312**, 170 (1998).
4. B. Yan, S. L. Chen, and P. C. Taylor, *MRS Symp. Proc.* **507**, 453 (1998).
5. S. L. Chen, J. M. Viner, and P. C. Taylor, *MRS Symp. Proc.* **507**, 459 (1998).
6. R. M. Mehra, I. Kaur, P. C. Mathur, and P. C. Taylor, *J. Non-Cryst. Solids* **227-230**, 243 (1998).
7. B. Yan, J. H. Dias da Silva, and P. C. Taylor, *J. Non-Cryst. Solids* **227-230**, 528 (1998).
8. P. C. Taylor, in *Properties of Amorphous Silicon and its Alloys*, T. Searle, ed. (INSPEC, London, 1998), p. 139.
9. B. Yan and P. C. Taylor, *MRS Symp. Proc.* **507**, 805 (1998).
10. N. Schultz, Z. V. Vardeny, and P. C. Taylor, *MRS Symp. Proc.* **507**, 745 (1998).
11. P. C. Taylor, *Egypt. J. Phys.* (1998), in press.
12. S. Chen and P. C. Taylor, *MRS Symp. Proc.* (1999), submitted.

<b>REPORT DOCUMENTATION PAGE</b>			Form Approved OMB NO. 0704-0188	
Public reporting burden for this collection of information is estimated to average 1 hour per response, including the time for reviewing instructions, searching existing data sources, gathering and maintaining the data needed, and completing and reviewing the collection of information. Send comments regarding this burden estimate or any other aspect of this collection of information, including suggestions for reducing this burden, to Washington Headquarters Services, Directorate for Information Operations and Reports, 1215 Jefferson Davis Highway, Suite 1204, Arlington, VA 22202-4302, and to the Office of Management and Budget, Paperwork Reduction Project (0704-0188), Washington, DC 20503.				
1. AGENCY USE ONLY (Leave blank)		2. REPORT DATE October 1999	3. REPORT TYPE AND DATES COVERED Phase I Annual Technical Progress Report, January 1998 – January 1999	
4. TITLE AND SUBTITLE Characterization of Amorphous Silicon Thin Films and PV Devices; Phase I Annual Technical Progress Report, January 1998 – January 1999			5. FUNDING NUMBERS C: XAK-8-17619-13 TA: PV005001	
6. AUTHOR(S) P.C. Taylor , G.A. Williams, W.D. Ohlsen , J.M. Viner, S.L. Chen, N. Schultz, T. Su, and W. Xu				
7. PERFORMING ORGANIZATION NAME(S) AND ADDRESS(ES) Department of Physics University of Utah Salt Lake City, UT 84112			8. PERFORMING ORGANIZATION REPORT NUMBER	
9. SPONSORING/MONITORING AGENCY NAME(S) AND ADDRESS(ES) National Renewable Energy Laboratory 1617 Cole Blvd. Golden, CO 80401-3393			10. SPONSORING/MONITORING AGENCY REPORT NUMBER SR-520-27298	
11. SUPPLEMENTARY NOTES NREL Technical Monitor: B. von Roedern				
12a. DISTRIBUTION/AVAILABILITY STATEMENT National Technical Information Service U.S. Department of Commerce 5285 Port Royal Road Springfield, VA 22161			12b. DISTRIBUTION CODE	
13. ABSTRACT (Maximum 200 words) Major accomplishments of the previous year include (1) an evaluation of the potential for n-type doping of a-SiS <sub>x</sub> :H and a-SiSe <sub>x</sub> :H alloys, (2) an investigation of the optically induced metastabilities in a-SiS <sub>x</sub> :H and a-SiSe <sub>x</sub> :H alloys with regard to their potential use in photovoltaic applications, and (3) a more detailed understanding of the kinetics of light-induced electron spin resonance (ESR) due to carriers trapped in localized band-tail states in a-Si:H. Also of importance are preliminary measurements of the defects and metastabilities in hot-wire samples of a-Si:H and in samples of a-Si:H made under strong hydrogen dilution. The preliminary measurements on hydrogen dilution suggest that the production of neutral silicon dangling bonds is not suppressed from the standard material even though there appears to be an improvement in the stability of cells made using the hydrogen-dilution process. The new three-chamber, load-locked plasma-enhanced chemical vapor deposition system is functioning and producing intrinsic and doped films of a-Si:H. Plans for the next year include the production of high quality devices using this new deposition system.				
14. SUBJECT TERMS photovoltaics ; amorphous silicon ; thin films ; photovoltaic devices ; electron spin resonance ; light-induced defects ; low-temperature kinetics ; band-tail carriers ; nuclear magnetic resonance ; plasma-enhanced chemical vapor deposition			15. NUMBER OF PAGES	
			16. PRICE CODE	
17. SECURITY CLASSIFICATION OF REPORT Unclassified	18. SECURITY CLASSIFICATION OF THIS PAGE Unclassified	19. SECURITY CLASSIFICATION OF ABSTRACT Unclassified	20. LIMITATION OF ABSTRACT UL	